ACS central science

Research Article

Cite This: ACS Cent. Sci. 2019, 5, 365−373

http://pubs.acs.org/journal/acscii

High-Performance Quasi-Solid-State MXene-Based Li−I Batteries

Xiao Tang,[†,⊥] Dong Zhou,[†,⊥] Peng Li,[‡] Xin Guo,[†] Chengyin Wang,[§] Feiyu Kang,[∥] Baohua Li,*[,∥] and Guoxiu Wang*[,†]

[†]Centre for Clean Energy Technology, Faculty of Science, University of Technology Sydney, Sydney, New South Wales 2007, Australia

[‡]College of Material Science and Engineering, Nanjing University of Aeronautics and Astronautics, Nanjing 210006, P. R. China

[§]College of Chemistry and Chemical Engineering, Yangzhou University, Yangzhou 225002, P. R. China

[∥]Key Laboratory of Thermal Management Engineering and Materials, Graduate School at Shenzhen, Tsinghua University, Shenzhen 518055, P. R. China

Supporting Information

ABSTRACT: Lithium−iodine (Li−I) batteries have attracted tremendous attention due to their high energy and power densities as well as the low cost of iodine. However, the severe shuttle effect of iodine species and the uncontrollable lithium dendrite growth have strongly hindered their practical applications. Here we successfully develop a quasi-solid-state Li−I battery enabled by a MXene-based iodine cathode and a composite polymer electrolyte (CPE) containing $NaNO_3$ particles dispersing in a pentaerythritol-tetraacrylate-based (PETEA-based) gel polymer electrolyte. As verified by experimental characterizations and first-principle calculations, the abundant functional groups on the surface of MXene sheets provide strong chemical binding to iodine species, and therefore immobilize their shuttling. The PETEA-based polymer matrix simultaneously suppresses the diffusion of iodine species and stabilizes the Li anode/CPE interface against dendrite growth. The $NaNO_3$ particles act as an effective catalyst to facilitate the transformation kinetics of LiI_3 on the cathode. Owing to such synergistic optimization, the as-developed Li−I batteries deliver high energy/power density with long cycling stability and good flexibility. This work opens up a new avenue to improve the performance of Li−I batteries.

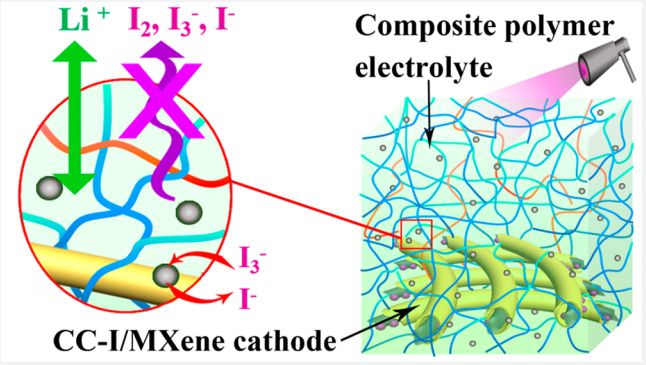

INTRODUCTION

In modern society, the development of new-generation rechargeable batteries with high energy density, high power density, and low cost is highly desired due to soaring demand for utilizing renewable energy and reducing air pollution.[1] As a promising alternative to lithium-ion (Li-ion) batteries, rechargeable lithium−iodine (Li−I) batteries based on a conversion mechanism ($I_2 + 2Li \leftrightarrow 2LiI$) have drawn intensive attention owing to their high theoretical capacity (1040 mA h cm^{-3} and 211 mA h g^{-1}), superior rate performance, degassing-free battery chemistry, and the low cost of iodine.[2,3] However, currently, the development of Li−I batteries has been stunted by many intrinsic obstacles. Iodine-based electrodes usually suffer from poor electrical conductivity of the elemental iodine (I_2).[4] More severely, iodine species (i.e., I_2, I_3^-, and I^-) are highly dissoluble in organic electrolyte solvents. This not only results in serious self-discharge due to their shuttle effect, but also leads to increased internal resistance together with decreased Li^+ transport kinetics.[5,6] Furthermore, uncontrollable dendrite growth on the Li anode during cycling deteriorates the Li/electrolyte interface and causes safety hazards.[7,8]

To improve the performance of Li−I batteries, many efforts have been devoted to confine iodine in carbon (C) matrices (such as graphene,[4,9] carbon microtubes,[10] porous carbon,[2,11,12] and heteroatom-doped carbon[13,14]) with the aim of enhancing electronic conductivity and suppressing the dissolution/diffusion of iodine species. However, the physical adsorption of iodine species in these carbon matrices is insufficient to prohibit the shuttle effect. Therefore, it is highly desired to develop a novel iodine-based cathode simultaneously possessing high iodine loading and strong chemical binding of iodine species. As for the electrolyte, replacing organic liquid electrolyte (LE) with solid electrolyte can synergistically restrain the diffusion of dissolved iodine species and eliminate safety issues (fire and explosion, etc.), which could result from the leakage of flammable electrolyte solvents.[15] However, the low ionic conductivity of solid electrolyte and the unstable electrode/solid electrolyte interface greatly limit their applications in Li−I batteries.

Received: December 11, 2018
Published: February 1, 2019

DOI: 10.1021/acscentsci.8b00921
ACS Cent. Sci. 2019, 5, 365−373

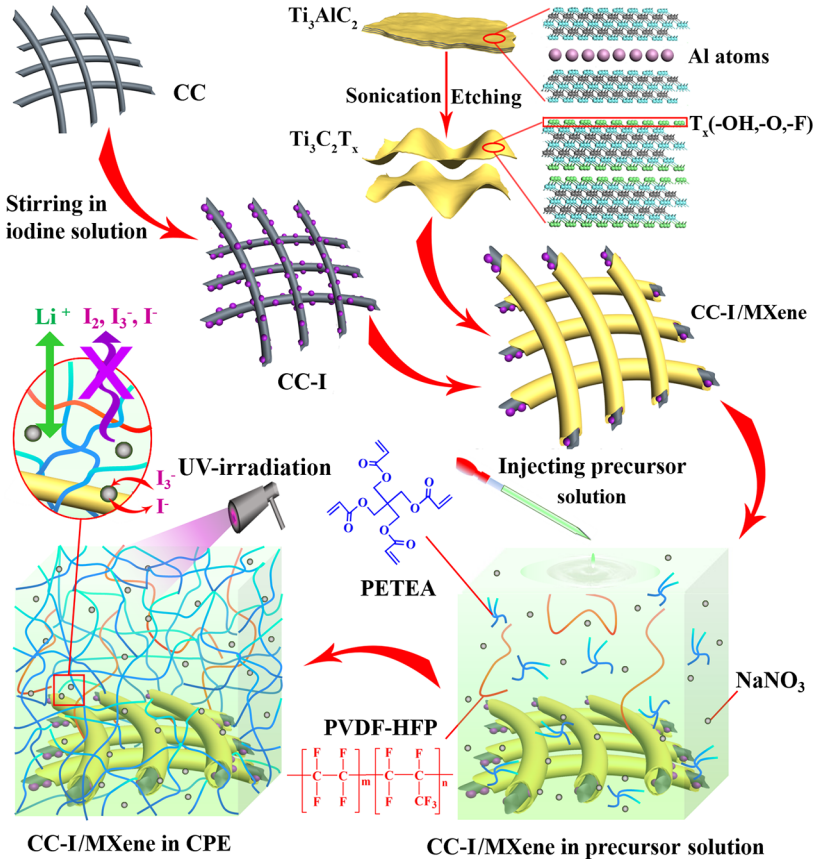

Figure 1. Schematic illustration of the preparation of MXene-wrapped carbon cloth−iodine cathodes and composite polymer electrolyte.

Recently, we have proposed a versatile technique for the preparation of MXene-based electrode materials,[16,17] and an intensive investigation on the liquid/polymer electrolytes[18−20] for conversion mechanism-based alkali metal batteries. Based on these, for the first time, we successfully develop a flexible quasi-solid-state Li−I battery integrated with a $Ti_3C_2T_x$ (T represents surface functional group, and x is number of such groups) MXene-wrapped carbon cloth−iodine (CC−I/MXene) cathode and a composite polymer electrolyte (CPE) composed of catalytic $NaNO_3$ particles dispersing in a pentaerythritol-tetraacrylate-based (PETEA-based) gel polymer electrolyte. As verified by theoretical calculations and experimental investigations, the $Ti_3C_2T_x$ MXene sheets with abundant surface functional groups can effectively confine the iodine species inside the cathode, and therefore restrain the shuttle effect. In the *in situ* prepared CPE, the PETEA-based polymer matrix can efficiently suppress the diffusion of iodine species, and benefit for the formation of a stable Li anode/CPE interface without dendrite growth. Meanwhile, the $NaNO_3$ particles not only greatly enhance the mechanical strength of CPE, but also effectively increase the kinetic transformation of LiI_3 on the cathode. The as-developed quasi-solid-state Li−I batteries exhibit a high energy density with stable cycling performance and excellent flexibility.

RESULTS AND DISCUSSIONS

Figure 1 illustrates the preparation of the Li|CPE|CC−I/MXene batteries. Iodine can be facilely loaded onto the porous carbon cloth (CC) by a simple "solution−adsorption" method to obtain the flexible carbon cloth−iodine (CC−I) electrodes. After the iodine-absorption, the specific surface area of carbon cloth significantly decreased, indicating a successful loading of iodine into the porous structure of carbon cloth (shown in Figure S1). Delaminated $Ti_3C_2T_x$ MXene was prepared by selectively etching Al atoms in Ti_3AlC_2 (MAX) precursor materials followed by sonication (Figure S2). By adopting a "drop-filtration" process, the CC−I electrodes can be tightly wrapped by the MXene sheets (Figure 1, upper panels), which can greatly improve the stability of iodine due to the strong interaction (Figure S3).

To further enhance the electrochemical performance of CC−I/MXene cathodes in batteries, optimization of electrolyte has been conducted. Based on previous research, it is believed that the addition of $LiNO_3$ in ether-based electrolytes benefits for the formation of a passive film on the Li anode, and therefore suppresses its corrosion from dissolved iodine species.[12] However, as shown in Figure S4, a Li anode precycled in a $LiNO_3$-containing liquid electrolyte (LE) cannot suppress the serious self-discharge, while Li−I cells using a suspension of insoluble $NaNO_3$ in LE can deliver a negligible self-discharge, which is comparable to that of the $LiNO_3$-containing LE. Therefore, we present a new understanding on the role of nitrates in Li−I batteries. We suggest that $NaNO_3$ can catalyze the conversion from I_3^- to elemental I_2 near the end of the charging process. Thus, we prepared a composite polymer electrolyte consisting of 2 wt % $NaNO_3$ homogeneously dispersing in a PETEA-based gel polymer electrolyte. First, $NaNO_3$ particles were dispersed in 1 M bis(trifluoromethane) sulfonamide lithium (LiTFSI) in 1,2-dioxolane (DOL):dimethoxymethane (DME) (1:1, v/v) electrolyte [in which a small amount of PVDF-HFP (poly(vinylidene fluoride-hexafluoropropylene)) was dissolved to

DOI: 10.1021/acscentsci.8b00921
ACS Cent. Sci. 2019, 5, 365−373

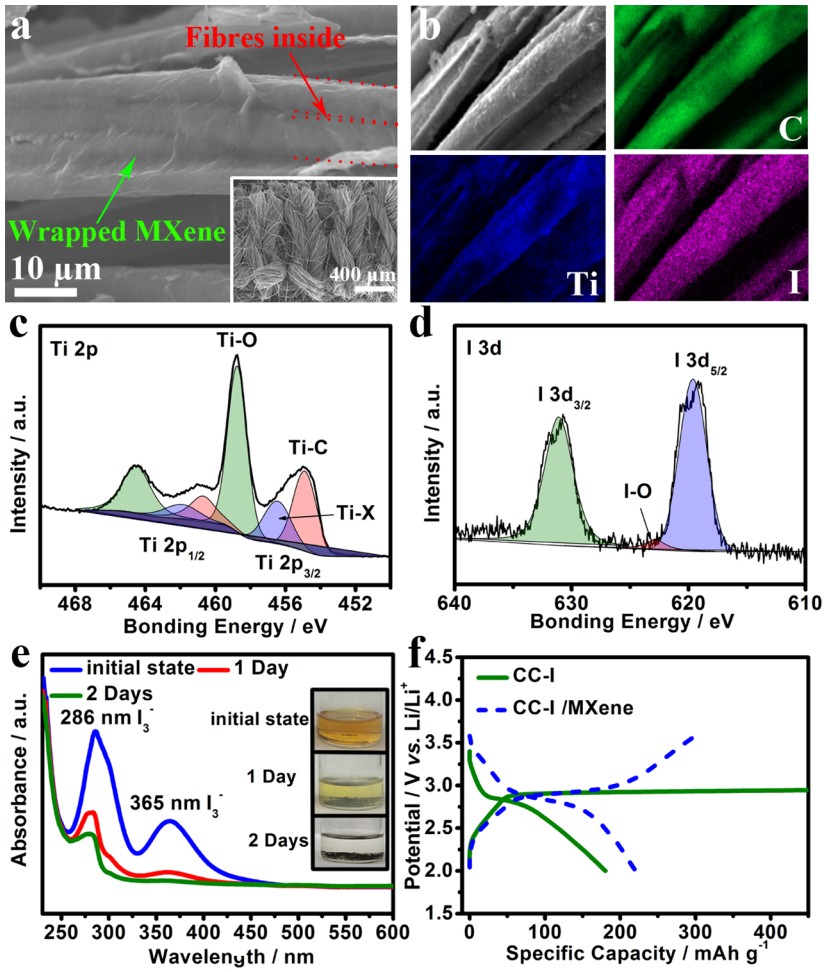

Figure 2. Characterizations of CC−I/MXene electrodes. (a) FE-SEM images and (b) EDS mappings of elemental Ti, C, and I on a CC−I/MXene electrode. High-resolution XPS spectra of (c) Ti 2p and (d) I 3d in a CC−I/MXene electrode. (e) UV−vis spectra and corresponding digital images of LiI_3 solution before and after loading MXene sheets. (f) Initial discharge/charge curves of Li|LE|CC−I and Li|LE|CC−I/MXene cells at 0.5 C.

improve the dispersion of $NaNO_3$ particles] to form a suspension, and then PETEA monomer together with 2-hydroxy-2-methyl-1-phenyl-1-propanone (HMPP) photoinitiator were dissolved into the suspension to obtain a precursor solution. After that, the precursor solution was subjected to ultraviolet-light-irradiation (UV-irradiation) to initiate a radical polymerization of C═C bonds on the monomers, and thereafter the cross-linked CPE was *in situ* constructed on the surface of the CC−I/MXene cathode (Figure 1, lower panels). In such CPE, the PETEA-based polymer matrix with strong chemical interaction with iodine species can efficiently suppress their shuttle effect and simultaneously stabilize the Li anode/CPE interface. Furthermore, $NaNO_3$ particles can not only greatly enhance the mechanical strength of the CPE (Figure S5), but also act as an effective catalyst on the iodine cathode/CPE interface. Such collaborative optimization on electrode and electrolyte is expected to achieve a superior cycling stability for the Li−I batteries.

As shown in Figure S6a, the carbon cloth shows a morphology of tidily knitted carbon fibers. No structural change is observed after absorbing iodine (Figure S6b). For the CC−I/MXene electrode, it is clearly seen that the iodine-loaded carbon fibers are well-wrapped by the MXene sheets (Figure 2a and Figure S7a,b). This is further confirmed by the uniform distribution of elemental titanium (Ti), carbon (C), and iodine (I) in the energy dispersive spectrometer (EDS) images of a CC−I/MXene electrode (Figure 2b). Furthermore, no characteristic peak of iodine can be observed in the X-ray diffraction (XRD) pattern (Figure S7c) and Raman spectrum (Figure S7d) of the MXene-wrapped electrode, indicating the formation of amorphous iodine during the solution−adsorption process, which is consistent with previous reports.[13] X-ray photoelectron spectroscopy (XPS) was applied to investigate the chemical composition of the CC−I/MXene electrode. The Ti 2p spectrum (Figure 2c) shows two Ti $2p_{3/2}$ doublets at 455.1 and 458.7 eV, and two Ti $2p_{1/2}$ doublets at 461.1 and 464.4 eV, respectively. As for the Ti $2p_{3/2}$, three deconvoluted peaks at 455.1, 456.5, and 458.7 eV can be assigned to Ti−C bonds, Ti-X bonds, and Ti−O surface bonds, respectively. Similarly, three deconvoluted peaks at 460.9, 461.9, and 464.4 eV are observed in the Ti $2p_{1/2}$.[16,21] Such a Ti 2p spectrum result confirms the successful wrapping of MXene sheets on the electrode without any compositional change. Figure 2d exhibits the XPS spectrum of I 3d in the CC−I/MXene electrode, in which peaks located at around 619.9 and 631.2 eV are associated with I $3d_{5/2}$ and I $3d_{3/2}$, respectively.[22] Noticeably, a peak located at around 623 eV can be ascribed to the chemical adsorption between iodine and the

DOI: 10.1021/acscentsci.8b00921
ACS Cent. Sci. 2019, 5, 365−373

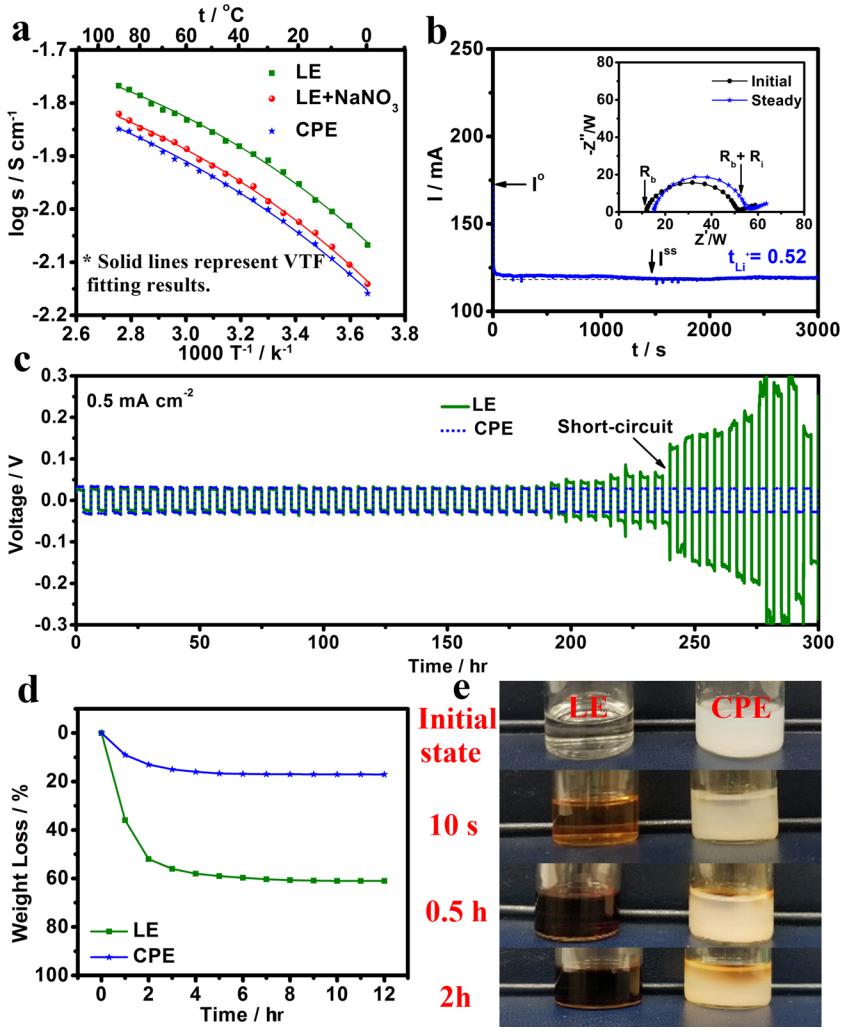

Figure 3. Characterizations of the CPE. (a) Ionic conductivities of 1 M LiTFSI in DOL:DME (1:1, v/v) LE, LE suspended with $NaNO_3$, and CPE as a function of temperature. The plots represent the experimental data, and meanwhile the solid lines represent VTF fitting results. (b) Chronoamperometry profile of a symmetric Li|CPE|Li cell under a polarization voltage of 10 mV. The corresponding EISs before and after the polarization are shown in inset. (c) Galvanostatic cycling curves of Li|Li symmetrical cells using LE or CPE at a current density of 0.5 mA cm^{-2} with cutoff capacity of 1.5 mA h cm^{-2}. (d) Weight loss of LE and CPE along with aging time at 25 °C. (e) Visual observation of iodine dissolution/diffusion in LE and CPE with different aging times.

−O/−OH terminations of MXene.[22] Such chemical bonding is further validated by the O 1s XPS spectrum (Figure S8). The interaction between iodine and the −O/−OH terminations is expected to confine the iodine in the cathode and suppress its dissolution. To estimate the adsorption ability of MXene for iodides, ultraviolet−visible (UV−vis) spectra of a 2 mL 0.005 M LiI_3 (prepared by dissolving LiI and I_2 with a stoichiometric ratio of 1:1) DOL solution were measured. As shown in Figure 2e, after adding 1 mg of MXene, the characteristic peaks of I_3^- at around 286 and 365 nm[23] decrease gradually with the aging time. After 2 days adsorption, the solution turned clear (the inset in Figure 2e), which illustrates a strong adsorption of iodides by the MXene. The initial discharge/charge curves of Li−I cells using CC−I and CC−I/MXene electrodes in nitrate-free LE (1 M LiTFSI in DOL/DME) are shown in Figure 2f. The CC−I cathodes show extremely low Coulombic efficiency and cannot be charged to above 3 V, which can be attributed to the severe shuttling of dissolvable iodine species. In sharp contrast, after wrapping with MXene sheets, the CC−I/MXene cathodes exhibit a significantly enhanced Coulombic efficiency (~73%) and reversible capacity (~219 mA h g^{-1}), indicating an effective immobilization of iodine species by the MXene sheets.

The Fourier transform infrared spectroscopy (FTIR) spectra of the PETEA monomer and the PETEA-based polymer matrix separated from CPE are shown in Figure S9, which verifies that the monomers have been successfully polymerized in the $NaNO_3$ suspension with a high degree of conversion. The ionic conductivities of the LE, LE suspended with $NaNO_3$, and CPE as a function of temperature from 0 to 90 °C are shown in Figure 3a. The plots of log σ versus T^{-1} for all electrolyte samples deliver a nonlinear relationship, which can be well-described by the Vogel−Tamman−Fulcher (VTF) empirical equation:[24]

$$\sigma = \sigma_0 T^{-1/2} \exp\left(-\frac{E_a}{R(T - T_0)}\right) \quad (1)$$

where E_a is the activation energy, σ_0 is the pre-exponential factor, R is the ideal gas constant, and T_0 is a parameter correlated to the glass transition temperature. It is worth noting that the E_a value (which indicates the barrier for ionic

DOI: 10.1021/acscentsci.8b00921
ACS Cent. Sci. 2019, 5, 365−373

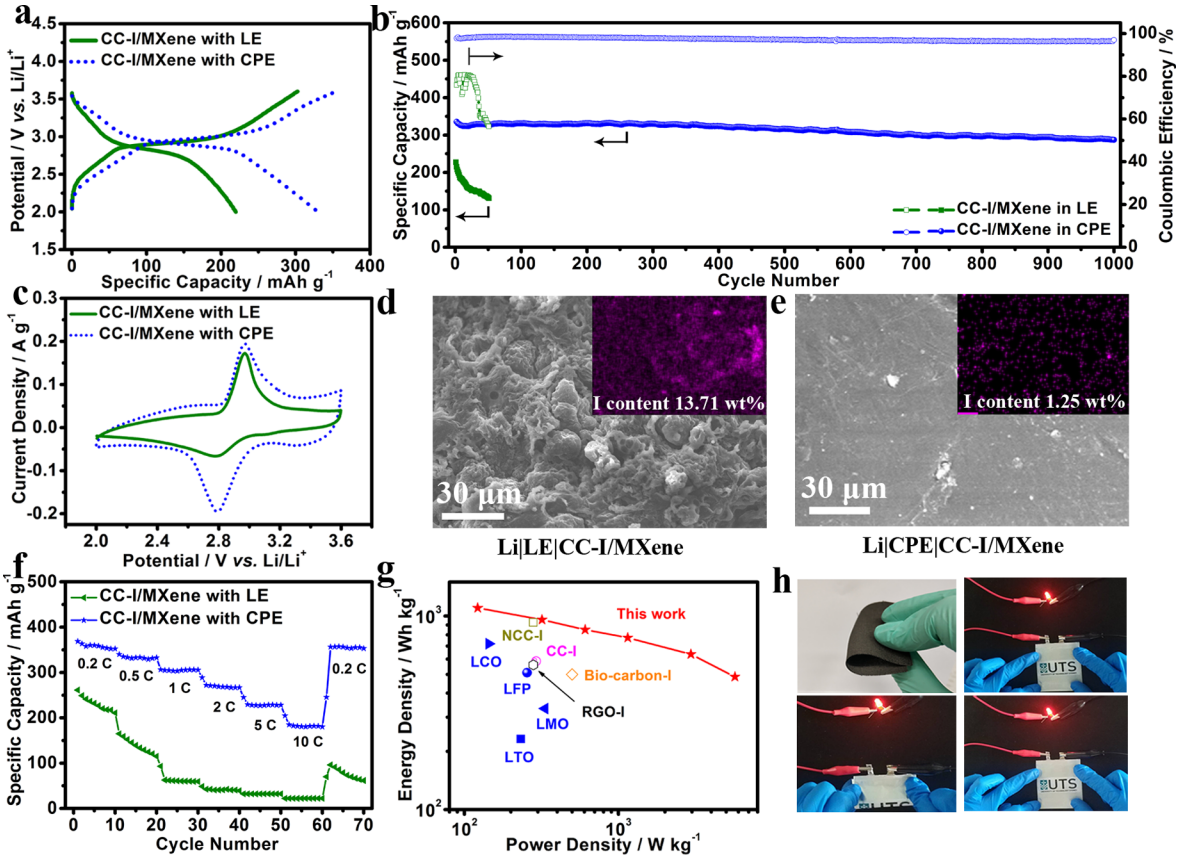

Figure 4. Electrochemical characterizations of Li−I cells. (a) Initial charge/discharge curves and (b) cycling performances of Li|LE|CC−I/MXene and Li|CPE|CC−I/MXene cells at 0.5 C. (c) CV curves at 0.1 mV s^{-1}. Morphologies and corresponding EDS mappings of iodine (shown in insets) of Li anodes obtained from the (d) Li|LE|CC−I/MXene and (e) Li|CPE|CC−I/MXene cells after 50 cycles at 0.5 C. (f) Rate performances of the above two Li−I cells. (g) Ragone plot of the as-assembled Li|CPE|CC−I/MXene battery compared with previously reported Li−I batteries[4,11−13] (open symbols) and representative Li-ion batteries[33] (solid symbols). (h) Digital images of an as-prepared CC−I/MXene cathode (upper left), and a red LED powered by a flexible Li|CPE|CC−I/MXene cell under flat−bent−flat states.

conduction) for the CPE obtained from the VTF fitting (8.92×10^{-3} eV) is quite close to that for the LE (7.37×10^{-3} eV, Table S1), indicating that, in the CPE, the adverse influence from small amounts of nonconductive additive components (i.e., polymers and $NaNO_3$) on ionic conduction is negligible. As a result, the CPE shows an extremely high conductivity of 9.50×10^{-3} S cm^{-1} at 25 °C, which is almost the same as that of the LE (1.18×10^{-2} S cm^{-1} at 25 °C). Such a high ionic conductivity value is sufficient to meet the requirement for Li−I batteries with high power density.

The Li-ion transference number (t_{Li}^+) is a crucial parameter for electrolytes, since a low t_{Li}^+ results in an increase in electrode polarization.[25] It is seen that the t_{Li}^+ of CPE reaches 0.52 (Figure 3b), which is much higher than that of the LE (0.23, Figure S10). This can be ascribed to the fact that the polymerized PETEA framework significantly immobilizes the anions.[18] Such enhanced t_{Li}^+ is expected to not only diminish the polarization of batteries, but also restrain the dendrite growth on Li anodes.[26] This is confirmed by galvanostatic cycling measurements on a symmetric Li|Li cell at a current density of 0.5 mA cm^{-2}. For the Li|LE|Li cell, the voltage hysteresis between the voltages of Li stripping and plating dramatically increases after ∼240 h, demonstrating a deteriorated Li/LE interface, resulting from an accumulated thick solid electrolyte interface (SEI) and Li dendrite growth (Figure 3c).[27] The Li|CPE|Li cell, in sharp contrast, delivers a much lower voltage fluctuation and maintains stability up to 300 h. This validates a uniform Li deposition with a stable Li/CPE interface. Therefore, the safety risks caused by dendrite growth have been successfully mitigated.

The durability and safety of the CPE are elucidated by measuring its weight loss in an open environment as a function of aging time at room temperature. As shown in Figure 3d, the CPE exhibits a slight weight loss with aging time (17 wt % after 12 h) due to the volatilization of electrolyte solvent, which is much lower than that of the LE (61 wt % after 12 h). Therefore, the CPE shows a much enhanced safety characteristic compared to LE. To directly characterize the dissolution and diffusion of iodine species in electrolytes, we performed visual observation on the same amount of iodine powder soaked in LE and CPE. The LE immediately turns dark brown after adding the iodine (Figure 3e, left), implying that the iodine powder massively dissolves in the LE. However, the CPE remains milky white with a light-yellow skin layer during the aging process (Figure 3e, right), indicating that the dissolution of iodine has been significantly alleviated in the CPE.

To investigate the electrochemical characteristics of the as-assembled Li−I batteries, the performances of CC−I/MXene electrodes using LE, $NaNO_3$-containing LE, and CPE were tested. As shown from the self-discharge phenomena (Figure S11), the potential of the Li|LE|CC−I/MXene cell decreases

DOI: 10.1021/acscentsci.8b00921
ACS Cent. Sci. 2019, 5, 365−373

rapidly due to the dissolution of active material and shuttle effect, while the cell with CPE achieves a negligible self-discharge after aging for 48 h, indicating the strong immobilization of iodine species by the CPE. The Li|LE|CC−I/MXene cell can deliver an initial discharge capacity of 219 mA h g^{-1} (based on the mass of iodine) at 0.5 C with a Coulombic efficiency of 73% (Figure 4a). It should be noticed that such a capacity value is higher than the theoretical capacity of Li−I batteries (211 mA h g^{-1}), since the MXene sheets as well as porous carbon cloth substrates can also impart capacity due to the capacitive behavior (Figure S12). After adding $NaNO_3$ into the LE, an enhanced capacity (301 mA h g^{-1}) and Coulombic efficiency (~92%) are achieved at 0.5 C, suggesting that $NaNO_3$ can greatly enhance the transformation kinetics due to catalytic effect (Figure S13a). The capacity of CC−I/MXene electrodes in Li−I batteries can be further improved to ~330 mA h g^{-1} at 0.5 C by using CPE, since the cross-linked monomers in electrolyte can effectively immobilize the iodine species and prevent loss of active materials. The Li|CPE|CC−I/MXene cells also exhibit superior long-term cycling stability with 85% capacity retention after 1000 cycles, which is much higher than those with LE (57%, 50 cycles) and $NaNO_3$-containing LE (67%, 1000 cycles) (Figure 4b and Figure S13b).

Cyclic voltammetry (CV) was also performed for understanding the chemistry of Li|LE|CC−I/MXene, Li|LE+$NaNO_3$|CC−I/MXene, and Li|CPE|CC−I/MXene cells. As shown in Figure 4c and Figure S13c, a Li−I cell with the $NaNO_3$-containing LE exhibits enhanced current density and reduced potential gap between the main anodic and cathodic peaks than that of the cell with the LE, which indicates the catalytic effect of $NaNO_3$ particles. Moreover, the Li−I cell using CPE shows the highest peak current density, signifying a lower polarization contributed by the synergistic optimization of the catalytic $NaNO_3$ and PETEA-based polymer matrix. For the Li|CPE|CC−I/MXene cells, the capacity contribution from different behaviors can be studied by analyzing the CV curves at different scan rates. By applying the capacity separation method,[6] the noncapacitive capacity contribution can be obtained as displayed in the shadowed area of the CV curve (Figure S14). It is seen that, during the cathodic scan, a small hump emerges at ~3.3 V vs Li/Li^+, indicating the conversion of I_2 to I_3^-. The peak at ~2.8 V can be assigned to the reaction from I_3^- to I^-. The anodic scan is a reversible process, in which the peak at ~3.0 V indicates that I^- was oxidized to I_3^-, and I_3^- was further oxidized to I_2 at ~3.3 V.[4] Noticeably, the current sharply increased from ~3.5 V vs Li/Li^+, which could be attributed to the oxidation of the NO_3^- anions, as described in the following equation:[28]

$$NO_3^- - e \rightarrow NO_3 \quad (2)$$

Such NO_3 has been reported to widely exist in nature with a short life-span,[28,29] and usually forms as a reaction intermediate in electrochemical synthesis.[30] It is speculated that, in Li−I batteries, the NO_3 radicals tend to be consumed instantly by the I_3^- anions as described in the following equation:

$$2NO_3 + 2I_3^- \rightarrow 2NO_3^- + 3I_2 \quad (3)$$

Thus, $NaNO_3$ as the catalyst can effectively enhance the conversion kinetics and the transformation of I_3^- to I_2. This is well consistent with the corresponding *ex situ* Raman spectra in Figure S15a, in which the Raman peak of I_3^- (at ~120 cm^{-1})[31,32] disappears at the end of the charge process (3.6 V), demonstrating a complete oxidation of I_3^- to I_2. For comparison, due to poor kinetics, the peak of I_3^- in the Li|LE|CC−I/MXene cell still exists at the end of the charge process, which means that I_3^- cannot fully revert to I_2 (Figure S15b), resulting in the limited Coulombic efficiency as shown in Figure 4a.

Electrochemical impedance spectroscopy (EIS) was conducted to further investigate the interfacial behavior and reversibility of Li−I cells. Figure S16a,b presents the EIS results for Li−I cells after different cycles at 0.5 C. The EIS spectra can be well-simulated via an equivalent circuit as shown in Figure S16c, and the simulation results are summarized in Table S2. For the Li|LE|CC−I/MXene cell, the solid electrolyte interface resistance (R_f) sharply rises from 98.1 to 187.2 Ω after 50 cycles, which correlates with the unstable SEI film and dendrite growth on the anode as well as the severe shuttle effect in the cathode.[19] In sharp contrast, after replacing the LE with CPE, the values of R_f are much lower (21.7 Ω after 1 cycle), and maintain steady with limited variation during cycling (40.0 Ω after 50 cycles). This implies an inhibition of the shuttle of iodine species and a stable electrode/CPE interface, which contribute to the significantly improved cycling performance in Figure 4b. The Li anodes disassembled from Li−I cells after 50 cycles were observed by FE-SEM. Massive dendrite structures and microsized precipitates can be found on the surface of the Li anode disassembled from the Li|LE|CC−I/MXene cell, and the iodine content on such an anode is as high as 13.71 wt % (Figure 4d, corresponding to the digital image in Figure S17). The Li anode from the Li|LE+$NaNO_3$|CC−I/MXene cell shows an iodine content of 6.92 wt % (Figure S13e). With the CPE, the surface of the Li anode tends to be smooth, and the growth of Li dendrite has been remarkably suppressed. The iodine content of this Li anode is as low as 1.25 wt % (Figure 4e), confirming the successful suppression of the shuttle effect.

The rate performances of Li−I batteries are shown in Figure 4f and Figure S13d. Meanwhile, the corresponding voltage profiles are presented in Figure S18. The Li|CPE|CC−I/MXene cell delivered specific capacities of 358, 332, 303, 268, and 227 mA h g^{-1} at 0.2, 0.5, 1, 2, 5 C, respectively. Even at a high current density of 10 C, the cell can still maintain a capacity of 182 mA h g^{-1}, which is higher than Li|LE|CC−I/MXene and Li|LE+$NaNO_3$|CC−I/MXene cells. These values are also higher than those of Li|CPE|CC−I cells (Figure S19), and comparable to those of Li−I cells using the CC−I/MXene electrode and $LiNO_3$-containing polymer electrolyte (Figure S20). Furthermore, the charge/discharge potential gap of the cell with CPE is smaller than that of the cell with LE, which agrees very well with CV curves in Figure 4c. Li|CPE|CC−I/MXene cells with different areal mass loadings of iodine in the cathodes were further cycled at 0.5 C. With high iodine loadings of 7.5 and 10 mg cm^{-2}, the cell still can achieve capacities of 243 and 160 mA h g^{-1} after 350 cycles, respectively (Figure S21). Ragone plots (Figure 4g) have been used to compare the power densities and energy densities of the as-developed Li|CPE|CC−I/MXene battery with previously reported Li−I batteries and representative Li-ion batteries.[33] Obviously, the novel MXene-based Li−I battery delivers high energy densities (1050 W h kg^{-1} at 0.2 C and 485 W h kg^{-1} at 10 C) and power densities (125 W kg^{-1} at 0.2 C and 5700 W kg^{-1} at 10 C; Table S3), which are much higher

DOI: 10.1021/acscentsci.8b00921
ACS Cent. Sci. 2019, 5, 365−373

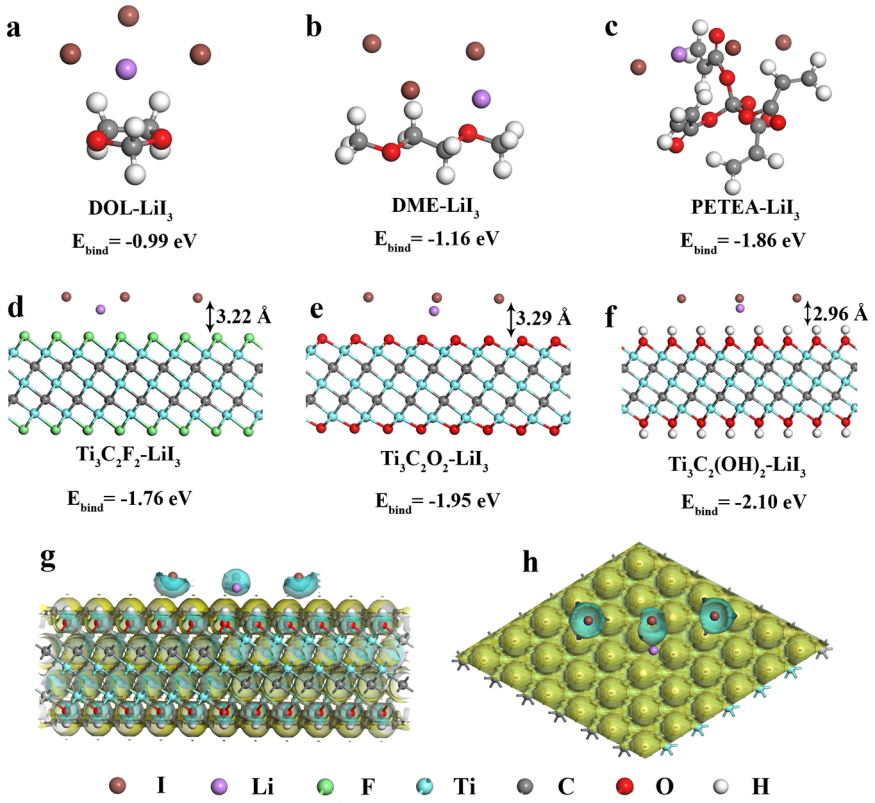

Figure 5. Theoretical calculations. Molecular models and calculated binding energies of LiI_3 with (a) DOL, (b) DME, and (c) PETEA monomer, and (d) $Ti_3C_2F_2$, (e) $Ti_3C_2O_2$, and (f) $Ti_3C_2(OH)_2$ as $Ti_3C_2T_x$ MXenes. (g) Side view and (h) top view of the difference in charge density for the optimized structure of LiI_3 adsorbed on $Ti_3C_2(OH)_2$ MXene. Yellow and blue indicate the charge depletion and accumulation, respectively.

than most of the previously reported Li−I batteries and lithium-ion batteries.

To explore the potential application of the CC−I/MXene electrode and CPE in flexible devices, a soft packed Li−I battery was fabricated (Figure 4h). The Li|CPE|CC−I/MXene battery can readily power a red light-emitting diode (LED) lamp under a repeated flat−bent−flat test. This demonstrates that the CC−I/MXene electrode can maintain structural integrity, and the electrode/CPE interfaces can keep tight adhesion under a dramatic shape deformation.

Theoretical calculations were conducted to further investigate the interaction between iodides (LiI_3 was selected as a representative of iodides) and MXenes as well as electrolyte. Figure 5a,b reveals that the binding energies of DOL-LiI_3 and DME-LiI_3 are calculated to be −0.99 and −1.16 eV, respectively, which are stronger than that of graphene−LiI_3 (−0.79 eV).[10] Thus, the LiI_3 molecules prefer to dissolve into these electrolyte solvents and shuttle to the anode. In contrast, the binding energy of PETEA−LiI_3 is around −1.86 eV. Consequently, LiI_3 molecules are preferentially immobilized by the functional groups in the polymer matrix of CPE, leading to its low solubility and slow diffusion in the CPE. This is highly consistent with the experimental results shown in Figure 3e. Furthermore, as shown in Figure 5d−f, binding energies of LiI_3 with $Ti_3C_2T_x$ MXenes [−1.76 eV for $Ti_3C_2F_2$ (Figure 5d), −1.95 eV for $Ti_3C_2O_2$ (Figure 5e), and −2.1 eV for $Ti_3C_2(OH)_2$ (Figure 5f)] are also much stronger than those of LiI_3 with electrolyte solvents, indicating that LiI_3 molecules prefer to adhere to the cathode/CPE surface rather than dissolve into the electrolyte. Notably, the difference in charge density of LiI_3 adsorbed on $Ti_3C_2T_x$ MXenes (Figure 5g,h and Figure S22) shows apparent charge transfer from MXenes to LiI_3, verifying the strong chemical interactions between LiI_3 and MXene, which leads to the enhanced binding energy as mentioned above. Therefore, the above-mentioned theoretical calculation results convincingly prove that MXene and CPE can cooperatively suppress the shuttle of iodine species and therefore improve the performance of Li−I batteries.

CONCLUSION

In summary, we have discovered that the synergistic optimization of a CC−I/MXene cathode in conjunction with a composite polymer electrolyte can significantly suppress the self-discharge and enhance the reversible capacity of Li−I batteries. The MXene sheets wrapped on the CC−I electrode possess a high binding energy with iodine species, which successfully restrains them in the cathode. The PETEA-based polymer matrix in the *in situ* prepared CPE not only immobilizes the iodine species against dissolution and diffusion, but also forms a stable Li anode/CPE interface to suppress the growth of Li dendrites. $NaNO_3$ particles act as a catalyst to efficiently improve the Coulombic efficiency of batteries by enhancing the transformation kinetics of LiI_3 in the cathode, and also improve the mechanical strength of CPE. The CC−I/MXene and CPE cooperatively enable a quasi-solid-state Li−I battery with high energy/power density, excellent cycling performance, and good flexibility. This work opens a new path to inspire the development of high-performance Li−I batteries and other novel Li-based rechargeable batteries (e.g., Li−oxygen, Li−sulfur, and Li−selenium batteries).

DOI: 10.1021/acscentsci.8b00921
ACS Cent. Sci. 2019, 5, 365−373

■ ASSOCIATED CONTENT

Supporting Information

The Supporting Information is available free of charge on the ACS Publications website at DOI: 10.1021/acscentsci.8b00921.

Detailed experimental procedures and additional materials characterization (PDF)

■ AUTHOR INFORMATION

Corresponding Authors

*E-mail: libh@sz.tsinghua.edu.cn.

*E-mail: Guoxiu.Wang@uts.edu.au.

ORCID

Baohua Li: 0000-0001-5559-5767

Guoxiu Wang: 0000-0003-4295-8578

Author Contributions

⊥Author X.T. and D.Z. contributed equally to this work.

Notes

The authors declare no competing financial interest.

Safety statement: no unexpected or unusually high safety hazards were encountered.

■ ACKNOWLEDGMENTS

This work was financially supported by the Australian Renewable Energy Agency (ARENA) Project (ARENA 2014/RND106) and the Australian Research Council (ARC) through the ARC Discovery Project (DP170100436). We thank Professor Yury Gogotsi (A.J. Drexel Nanomaterials Institute and Department of Materials Science and Engineering, Drexel University, Philadelphia, PA 19104, USA) for providing MAX phase Ti_3AlC_2 materials.

■ REFERENCES

(1) Schmuch, R.; Wagner, R.; Hörpel, G.; Placke, T.; Winter, M. Performance and cost of materials for lithium-based rechargeable automotive batteries. *Nat. Energy* **2018**, *3*, 267−278.

(2) Wang, Y.; Sun, Q.; Zhao, Q.; Cao, J.; Ye, S. Rechargeable lithium/iodine battery with superior high-rate capability by using iodine-carbon composite as cathode. *Energy Environ. Sci.* **2011**, *4*, 3947−3950.

(3) Gong, D.; Wang, B.; Zhu, J.; Podila, R.; Rao, A. M.; Yu, X.; Xu, Z.; Lu, B. An iodine quantum dots based rechargeable sodium-iodine battery. *Adv. Energy Mater.* **2017**, *7*, 1601885.

(4) Kim, S.; Kim, S. K.; Sun, P.; Oh, N.; Braun, P. V. Reduced graphene oxide/LiI composite lithium ion battery cathodes. *Nano Lett.* **2017**, *17*, 6893−6899.

(5) Zhao, Y.; Wang, L.; Byon, H. R. High-performance rechargeable lithium-iodine batteries using triiodide/iodide redox couples in an aqueous cathode. *Nat. Commun.* **2013**, *4*, 1896.

(6) Su, Z.; Wei, Z.; Lai, C.; Deng, H.; Liu, Z.; Ma, J. Robust pseudocapacitive Li-I_2 battery enabled by catalytic, adsorptive N-doped graphene interlayer. *Energy Storage Materials* **2018**, *14*, 129−135.

(7) Su, D.; Zhou, D.; Wang, C.; Wang, G. Toward high performance lithium-sulfur batteries based on Li_2S cathodes and beyond: status, challenges, and perspectives. *Adv. Funct. Mater.* **2018**, *28*, 1800154.

(8) Zheng, G.; Lee, S. W.; Liang, Z.; Lee, H.-W.; Yan, K.; Yao, H.; Wang, H.; Li, W.; Chu, S.; Cui, Y. Interconnected hollow carbon nanospheres for stable lithium metal anodes. *Nat. Nanotechnol.* **2014**, *9*, 618−623.

(9) Zhang, Q.; Wu, Z.; Liu, F.; Liu, S.; Liu, J.; Wang, Y.; Yan, T. Encapsulating a high content of iodine into an active graphene substrate as a cathode material for high-rate lithium-iodine batteries. *J. Mater. Chem. A* **2017**, *5*, 15235−15242.

(10) Su, Z.; Tong, C.-J.; He, D.-Q.; Lai, C.; Liu, L.-M.; Wang, C.; Xi, K. Ultra-small B_2O_3 nanocrystals grown in situ on highly porous carbon microtubes for lithium-iodine and lithium-sulfur batteries. *J. Mater. Chem. A* **2016**, *4*, 8541−8547.

(11) Wang, H.; Zhang, G.; Ke, L.; Liu, B.; Zhang, S.; Deng, C. Understanding the effects of 3D porous architectures on promoting lithium or sodium intercalation in iodine/C cathodes synthesized via a biochemistry-enabled strategy. *Nanoscale* **2017**, *9*, 9365−9375.

(12) Zhao, Q.; Lu, Y.; Zhu, Z.; Tao, Z.; Chen, J. Rechargeable lithium-iodine batteries with iodine/nanoporous carbon cathode. *Nano Lett.* **2015**, *15*, 5982−5987.

(13) Lu, K.; Hu, Z.; Ma, J.; Ma, H.; Dai, L.; Zhang, J. A rechargeable iodine-carbon battery that exploits ion intercalation and iodine redox chemistry. *Nat. Commun.* **2017**, *8*, 527.

(14) Li, K.; Lin, B.; Li, Q.; Wang, H.; Zhang, S.; Deng, C. Anchoring iodine to N-doped hollow carbon fold-hemisphere: toward a fast and stable cathode for rechargeable lithium-iodine batteries. *ACS Appl. Mater. Interfaces* **2017**, *9*, 20508−20518.

(15) Liu, F.-C.; Liu, W.-M.; Zhan, M.-H.; Fu, Z.-W.; Li, H. An all solid-state rechargeable lithium-iodine thin film battery using LiI (3-hydroxypropionitrile)$_2$ as an I^- ion electrolyte. *Energy Environ. Sci.* **2011**, *4*, 1261−1264.

(16) Bao, W.; Tang, X.; Guo, X.; Choi, S.; Wang, C.; Gogotsi, Y.; Wang, G. Porous cryo-dried MXene for efficient capacitive deionization. *Joule* **2018**, *2*, 778−787.

(17) Bao, W.; Liu, L.; Wang, C.; Choi, S.; Wang, D.; Wang, G. Facile synthesis of crumpled nitrogen-doped MXene nanosheets as a new sulfur host for lithium-sulfur batteries. *Adv. Energy Mater.* **2018**, *8*, 1702485.

(18) Zhou, D.; Chen, Y.; Li, B.; Fan, H.; Cheng, F.; Shanmukaraj, D.; Rojo, T.; Armand, M.; Wang, G. A stable quasi-solid-state sodium-sulfur battery. *Angew. Chem., Int. Ed.* **2018**, *57*, 10168−10172.

(19) Liu, M.; Zhou, D.; He, Y.-B.; Fu, Y.; Qin, X.; Miao, C.; Du, H.; Li, B.; Yang, Q.-H.; Lin, Z. Novel gel polymer electrolyte for high-performance lithium-sulfur batteries. *Nano Energy* **2016**, *22*, 278−289.

(20) Xu, X.; Zhou, D.; Qin, X.; Lin, K.; Kang, F.; Li, B.; Shanmukaraj, D.; Rojo, T.; Armand, M.; Wang, G. A room-temperature sodium-sulfur battery with high capacity and stable cycling performance. *Nat. Commun.* **2018**, *9*, 3870.

(21) Jiang, Q.; Kurra, N.; Alhabeb, M.; Gogotsi, Y.; Alshareef, H. N. All pseudocapacitive MXene-RuO_2 asymmetric supercapacitors. *Adv. Energy Mater.* **2018**, *8*, 1703043.

(22) Sherwood, P. M. X-ray photoelectron spectroscopic studies of some iodine compounds. *J. Chem. Soc., Faraday Trans. 2* **1976**, *72*, 1805−1820.

(23) Gardner, J. M.; Abrahamsson, M.; Farnum, B. H.; Meyer, G. J. Visible light generation of iodine atoms and I-I Bonds: sensitized I^- oxidation and I_3^- photodissociation. *J. Am. Chem. Soc.* **2009**, *131*, 16206−16214.

(24) Croce, F.; Focarete, M. L.; Hassoun, J.; Meschini, I.; Scrosati, B. A safe, high-rate and high-energy polymer lithium-ion battery based on gelled membranes prepared by electrospinning. *Energy Environ. Sci.* **2011**, *4*, 921−927.

(25) Zhou, D.; Liu, R.; Zhang, J.; Qi, X.; He, Y.-B.; Li, B.; Yang, Q.-H.; Hu, Y.-S.; Kang, F. In situ synthesis of hierarchical poly(ionic liquid)-based solid electrolytes for high-safety lithium-ion and sodium-ion batteries. *Nano Energy* **2017**, *33*, 45−54.

(26) Bai, P.; Li, J.; Brushett, F. R.; Bazant, M. Z. Transition of lithium growth mechanisms in liquid electrolytes. *Energy Environ. Sci.* **2016**, *9*, 3221−3229.

(27) Zhou, D.; Liu, R.; He, Y. B.; Li, F.; Liu, M.; Li, B.; Yang, Q. H.; Cai, Q.; Kang, F. SiO_2 hollow nanosphere-based composite solid electrolyte for lithium metal batteries to suppress lithium dendrite growth and enhance cycle life. *Adv. Energy Mater.* **2016**, *6*, 1502214.

(28) Zhang, S. S. A new finding on the role of $LiNO_3$ in lithium-sulfur battery. *J. Power Sources* **2016**, *322*, 99−105.

(29) Geyer, A.; Alicke, B.; Konrad, S.; Schmitz, T.; Stutz, J.; Platt, U. Chemistry and oxidation capacity of the nitrate radical in the

continental boundary layer near Berlin. *J. Geophys. Res.-Atmos.* **2001**, *106*, 8013−8025.
(30) Tomat, R.; Rigo, A. Electrochemical oxidation of aliphatic hydrocarbons promoted by inorganic radicals. II. NO_3 radicals. *J. Appl. Electrochem.* **1986**, *16*, 8−14.
(31) Štangar, U. L.; Orel, B.; Vuk, A. Š.; Sagon, G.; Colomban, P.; Stathatos, E.; Lianos, P. In situ resonance raman microspectroscopy of a solid-state dye-sensitized photoelectrochemical cell. *J. Electrochem. Soc.* **2002**, *149*, E413−E423.
(32) Jung, N.; Crowther, A. C.; Kim, N.; Kim, P.; Brus, L. Raman enhancement on graphene: adsorbed and intercalated molecular species. *ACS Nano* **2010**, *4*, 7005−7013.
(33) Manthiram, A. An outlook on lithium ion battery technology. *ACS Cent. Sci.* **2017**, *3*, 1063−1069.

DOI: 10.1021/acscentsci.8b00921
ACS Cent. Sci. 2019, 5, 365−373